



# Cyclic behavior of masonry walls retrofitted with post-installed twisted bars or bonded rebars

S. Cattaneo<sup>a,b,\*</sup>, P. Crespi<sup>a</sup>, M. Scamardo<sup>a</sup>, N. Vafa<sup>a</sup>

<sup>a</sup> ABC Department, Politecnico di Milano, Italy

<sup>b</sup> Construction Technologies Institute, Italian National Research Council (ITC-CNR), Italy

## ARTICLE INFO

### Keywords:

Masonry retrofitting  
Cyclic loading  
Bonded fastener  
Twisted bars  
Full-scale testing  
Wall to wall connections

## ABSTRACT

The damage observed after the recent earthquakes showed that the most common failures for masonry buildings involve out-of-plane mechanisms associated to the ineffective connection between walls. For this reason, retrofitting techniques aiming to achieve a box-like behavior are of great interest. This paper presents the results of an experimental study conducted to investigate two different retrofitting solutions used to improve the structural connection between orthogonal walls: a mechanical connection by means of twisted bars and a fastening solution with rebars and injection mortar. Two full-scale T-shaped masonry specimens were realized in solid clay brick, with a “weak” connection between the front and the back wall. The specimens were tested in unreinforced and strengthened configurations, considering different retrofitting layouts. An out-of-plane load was applied on the front wall, together with a vertical prestress to simulate the gravity load coming from the floors and walls above. Each specimen was tested in three consecutive runs: a monotonic one on the unreinforced masonry, a first cyclic run with the wall intersection reinforced with twisted bars, and a second cyclic run on the wall retrofitted with rebars and injection mortar, after the removal of the twisted bars. The twisted bar solution resulted in a significant increase of the dissipative capacity of the wall despite the number of adopted bars, while, in the case of rebars and adhesive, a higher resistance was achieved together with a perfect box-like behavior.

## 1. Introduction

The majority of historical and heritage buildings around the world consists of unreinforced masonry (URM). These structures were usually designed accounting for gravity loads only, without any specific consideration of seismic actions. For instance, in Italy, most of the masonry buildings, which in addition are often located in high seismic risk areas, were built before the introduction of the first seismic regulations [1,2].

The damage observed after past earthquakes proved the high vulnerability of URM structures with respect to the horizontal forces and the recorded human and economic losses have often been too high [3–6]. The seismic capacity of URM buildings is strictly related to the effectiveness of the structural connections between orthogonal walls and between walls and floors. When these connections are not effective, the “box” behavior of the building is not guaranteed and local failure mechanisms may develop as, for example, the detachment of outer walls with their overturning [7,8]. On the contrary, if the connections are properly designed, the response of the building is governed by in-plane

behavior of walls and its seismic capacity significantly increases.

For this reason, among all the available retrofitting solutions [9–13], the ones aimed at improving the box-like behavior of the buildings are of highest interest [14–17]. In this regard, the use of traditional steel ties has been very common in the past. However, more recently, post-installed fastening solutions [17,18], with steel or fiber reinforced polymer anchors, have become more and more popular thanks to their limited cost and easy application, especially if commercially available systems can be adopted. Despite the wide use of these techniques, very few experimental programs have been presented in scientific literature [15,17–21] and, even if technical codes stress the importance of providing effective connections during the seismic retrofit, no clear design approaches have been still proposed. Thus, so far, designers were left alone with the difficult task of complying with code requirements only supported by qualitative indications.

To fill this gap and help the designers, an experimental campaign on two full scale solid brick masonry T-shaped specimens was performed. The aim was to investigate the effectiveness of two different retrofitting solutions designed to improve the connection between orthogonal walls:

\* Corresponding author at: ABC Department, Politecnico di Milano, Italy.

E-mail address: [sara.cattaneo@polimi.it](mailto:sara.cattaneo@polimi.it) (S. Cattaneo).

a screw-type connection realized using twisted stainless-steel bars, and a bonded fasteners connection, both installed in pre-drilled holes. Despite the solution with bonded fasteners is often adopted in wall-to-wall connections, it has been investigated by other authors in very few occasions [15,21]. On the contrary, the helicoidal bars are usually adopted for other applications. In particular, they are often used to reinforce the bed joints in new masonry constructions and, more recently, they have been adopted as local repair (e.g., crack stitching) [22] or reinforcement of historical masonry [23,24].

With respect to the wall layout, the intersection between the front and the rear walls were specifically realized as “weak” to reproduce common execution practices. The test setup followed the provisions given by Maddaloni et al. in [15], considered as the most suitable to obtain the required information. Indeed, that experimental research had a very similar objective, investigating the behavior of a connection made with composite tubes, which could be an alternative system to those presented in this paper. The unreinforced walls were monotonically loaded out-of-plane until a first major crack was evident, associated with a load drop. After that, the specimens were unloaded, and the wall intersections were retrofitted using two different types of fasteners separately in two succeeding test runs. In the first run, 12 mm stainless-steel twisted bars were used in drill holes of 8 mm nominal diameter. In the second run, after removing the helicoidal bars, post-installed  $\varnothing 12$  mm rebars were installed with injection mortar into re-drilled holes of nominal diameter 14 mm. The out-of-plane load was applied cyclically in the upper part of the front wall and transferred to the rear wall by the connectors.

The paper presents the main findings observed in the experimental program, discussing the insights gained considering the recent developments in seismic qualification and design of fastenings to masonry [25–27].

## 2. Experimental research

### 2.1. Geometry and materials

The experimental research considered two full scale T-shaped masonry wall specimens (W1 and W2) assembled with the typical English bond layout, which is very popular in Italy. The geometry of the specimen aimed at reproducing common orthogonal bearing walls of existing masonry buildings. The length of the front and rear walls were 2.2 m and 1.37 m, respectively. The height of both walls was 2.11 m and the thickness 25 cm in 2 wythes (Fig. 1). The specimens were made of solid clay brick with dimensions of  $25 \times 12 \times 5.5$  cm. Cementitious mortar was used for the joints, with a thickness of about 10 mm. The mean compressive strength of the bricks was evaluated according to ASTM C67/C67M [28] and resulted in 23.3 MPa, while the splitting strength evaluated according to ASTM C1006/C1006M [29] resulted in 2.5 MPa. The mechanical properties of the mortar were obtained from splitting, bending and compressive tests according to BS1881-117, ASTM C348, ASTM C109 [30–32]. The splitting strength was 0.6 MPa, the bending strength was 2.0 MPa, and the compressive strength was 4.6 MPa.

To simulate a “weak” connection and trigger the failure in the T-joint, the English bond rule was modified according to Fig. 1, where only the blue bricks (layer A) bridge the two walls. The exception weakening the connection with respect to the English bond assembling rule is here represented by the modified layer C.

### 2.2. Retrofitting techniques

At first, the unreinforced walls were loaded until a cracking failure at the joint section between the front and the rear wall was achieved. Then, two different techniques were selected to retrofit the walls:

twisted bars: 12 mm stainless-steel (AISI 304) bars Hilti Heli-Brick in 8 mm pre-drilled hole [33];

post-installed 12 mm B450C carbon-steel ribbed rebar with adhesive Hilti HY270 in 14 mm pre-drilled hole [34].

The twisted bars (yielding load 16.1 kN, ultimate load 18.9 kN,

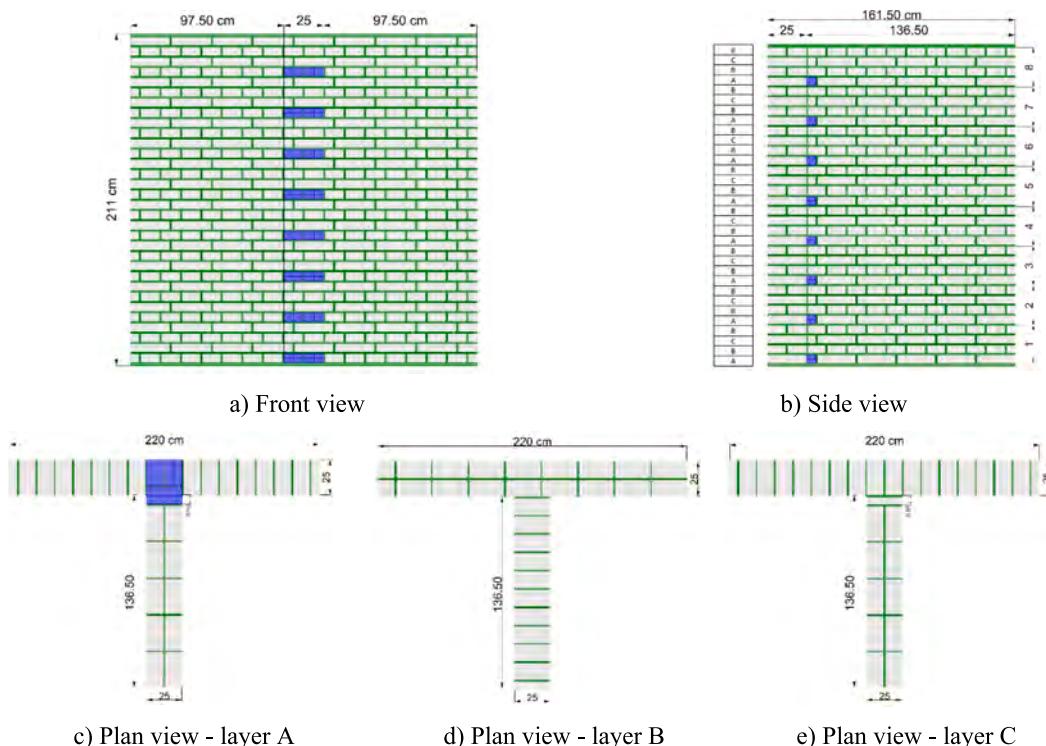


Fig. 1. Geometry of the specimens.

Young Modulus 122 GPa) were screwed in pre-drilled holes. The number of twisted bars was evaluated with the intention to increase the horizontal force from  $F_1$  (Fig. 2), associated to the detachment of the front wall from the rear one, up to the force  $F_3$  associated to the overturning of the whole structure. Considering the walls as located at the ground floor of a hypothetical three stories masonry building, a vertical prestress of about 0.2 MPa was assumed acting on top of the walls. By imposing the equilibrium of the structure, the theoretical forces  $F_1$ ,  $F_2$  and  $F_3$  resulted in 10 kN, 45 kN and 50 kN, respectively.

According to the experimental research presented by Cattaneo et al. in [35], a design pull-out load of about 3 kN was assumed for a single twisted bar, considering the installation in the middle of a brick. Therefore, about 16 twisted bars were calculated to equilibrate the force associated to the overturning failure mechanism. Eventually, one specimen was retrofitted with 16 bars distributed in pair on eight levels to maintain the symmetry of the pattern, while the other specimen was retrofitted with 8 bars only, to assess whether such a simpler and cheaper solution would still be effective. The final configurations of the two retrofitted walls with twisted bars are shown in Fig. 3. The total embedment depth was 85 cm (25 cm in the front wall and 60 cm in the rear wall). The anchors were placed at mid brick location of header bricks except for the area close to the horizontal loading beam, where some anchors were located in the vertical mortar joints.

Once the cyclic test was performed, all twisted bars were extracted and replaced by 8 post-installed rebars (12 mm, drill hole 14 mm) according to the distribution shown in Fig. 3a such that, in case of prior installation of 16 twisted bars, 8 locations were left free. In the first wall, the total embedment length of the rebars was 85 cm (as for twisted bar), while in the second specimen the total embedment length was 65 cm (25 cm in the front wall and 40 cm in the rear wall).

### 2.3. Test set-up

The tests were carried out by applying simultaneously the horizontal out-of-plane displacement on the front wall and a constant vertical load on all walls (prestress level 0.2 MPa). The latter aimed at reproducing the stress associated to the hypothetic gravity load given by three floors and two masonry levels placed on top of the specimen. Fig. 4 shows the test set-up. The specimens were connected to the strong floor with four threaded rods equipped with four load cells to monitor the prestress level. In the first specimen, the prestress was applied by screwing the rods, while in the second specimen, the rear wall was equipped with two jacks in order to maintain a constant prestress without efforts during the test execution.

A servo-hydraulic actuator with capacity of 300 kN (Fig. 4a) was located at the height of 172 cm above the floor to apply the horizontal load on the front wall. This measure was selected to maximize the lever arm of the horizontal load with respect to the ground and to fit the reaction frame of the laboratory, given the height of the specimen (211 cm). The point load was distributed along the width of the wall by means of a horizontal steel beam connected to the jack (Fig. 4b). Two additional horizontal steel beams, placed on the back side of the front wall (Fig. 4c), were connected to the front beam by mean of threaded rods to

transfer the applied load homogeneously to the whole specimen.

The absolute and relative displacements between the front and the back walls were recorded with numerous LVDTs (18 on specimen W1 and 20 on specimen W2) placed in different positions on the specimens, according to Fig. 5. Each sensor was associated with a code which reports, in order, the progressive numbering, the type of measure, and the position in cm with respect to the floor. The coded types of measurements are: the absolute displacement of the front wall (FR), the relative displacement between the back and the front wall on the right side (BR) and on the left side (BL), the absolute vertical (UV) and horizontal (UH) displacement of the back wall, the displacement along the diagonal of the back wall placed on the left side (D), the relative displacement between the front wall and the twisted bars 2 (H2) and 8 (H8) (see Fig. 3b).

All data in terms of loads and displacements were acquired using the HBM Spider 8 system at a sampling rate of 2 Hz.

### 2.4. Test procedure

The test procedure involved several steps. At first, after the specimen was positioned, a vertical prestress of 0.2 MPa was applied, which was increased up to 0.3 MPa only at the final stage of the test of specimen W2 retrofitted with rebars. Then, the monotonic test on the unreinforced specimen was performed by applying the load with the horizontal jack until a first crack was detected. The displacement associated to the peak load of the monotonic test (crack detection) was assumed as the First Major Event (FME), which was used as reference for the following cyclic tests.

After the monotonic test, the wall was retrofitted with twisted bars (8 in the wall W1 and 16 in the wall W2, see Fig. 3) and the cyclic test was performed by imposing increasing displacements with three cycles at the same magnitude and increasing steps of 25 % of the FME as shown in Fig. 6. To guarantee safety, the test was stopped when achieving too large displacements.

Once the specimen was unloaded, the twisted bars were pulled out with a hydraulic jack and the residual resistance was measured via a load-cell of 50 kN capacity. The displacement of the twisted bar was measured by two LVDT's with 100 mm gauge length, as depicted in Fig. 7 (left). The test was performed unconfined to evaluate the peak load. After that, due to the deep embedment length (85 cm), a hydraulic hollow jack was used to completely extract the bar in a confined setup (Fig. 7, right).

Eight holes according to the scheme of Fig. 3a were re-drilled with a nominal drill bit of 14 mm, and 12 mm rebars were installed with an injection mortar system as per the ETA of the product [34]. In specimen W1, the rebar embedment depth was 85 cm, while in specimen W2 it was reduced to 65 cm. The retrofitted specimen was subjected to increasing cyclic displacements with the same procedure adopted for the twisted bars. Again, to guarantee safety, the test was stopped when achieving too large displacements.

A summary of the performed tests is reported in Table 1.

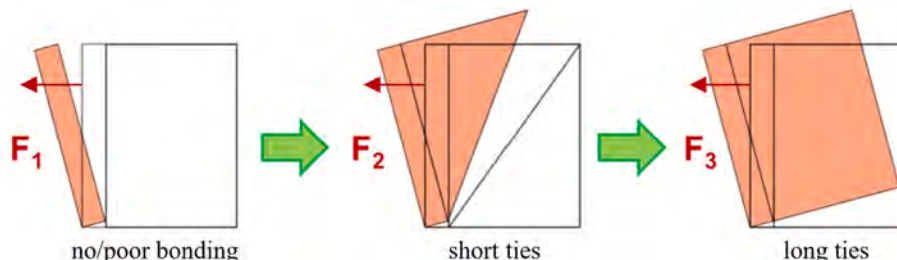


Fig. 2. Possible failure mechanisms.



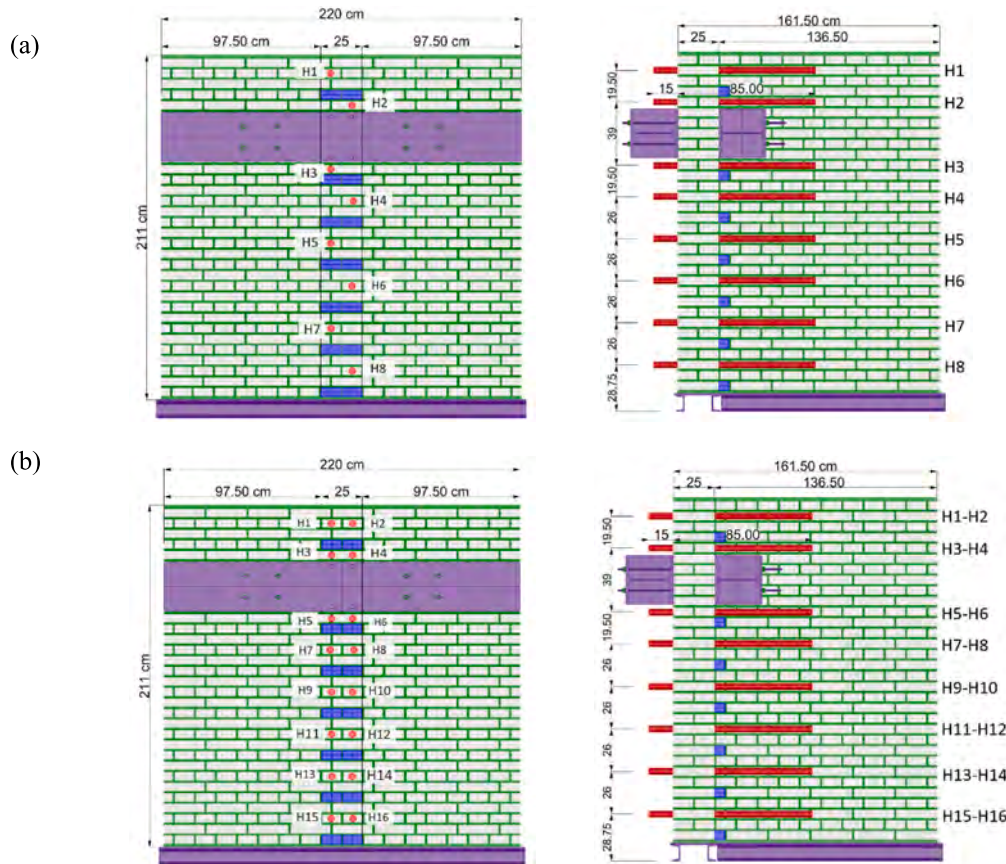


Fig. 3. Twisted bar position: (a) 8 bars and (b) 16 bars – measure in cm.

### 3. Experimental results

#### 3.1. Monotonic tests - unreinforced specimens

The specimens were subjected to a monotonically increasing displacement (0.03 mm/s) until the first crack was detected. Both specimens showed similar behavior with a crack at the intersection between the front and the rear wall, visible on both sides of the wall, and running from the top of the specimen down to about 50 cm from the bottom of the wall (Fig. 8).

The specimen W1 reached a maximum load of 49.5 kN, associated to a displacement of the jack (stroke) of 5.78 mm, which was defined as FME. Once the crack appeared, the load dropped suddenly to 30 kN as shown in the load–displacement curve (blue line) in Fig. 9. On the right axis, the vertical loads (front and back cells) are reported. The vertical load on the front wall load showed a limited variation (of about 3 kN, red line), while the vertical load of the rear wall progressively increased (up to 20 kN, green line) during the test, until a sudden drop associated to the FME occurred (from 73 kN to 59 kN). In the meantime, a certain uplift (up to 1.8 mm associated to the peak load) was noticed as shown in Fig. 9b, where the load and vertical uplift are plotted on the left and right axis vs time. Once the vertical crack between the front and rear wall appeared, a sudden drop occurred, and at the end of the monotonic test the specimen did not show any toe damage. A similar behavior was observed for the specimen W2.

#### 3.2. Cyclic test – Twisted bar reinforcement

Specimen W1 was retrofitted with 8 twisted bars, while specimen W2 was retrofitted with 16 bars as described in section §2.2 (see Fig. 3a and b, respectively). During the tests, no additional cracks developed in any specimen, while the existing cracks opened again during cycles (Fig. 10).

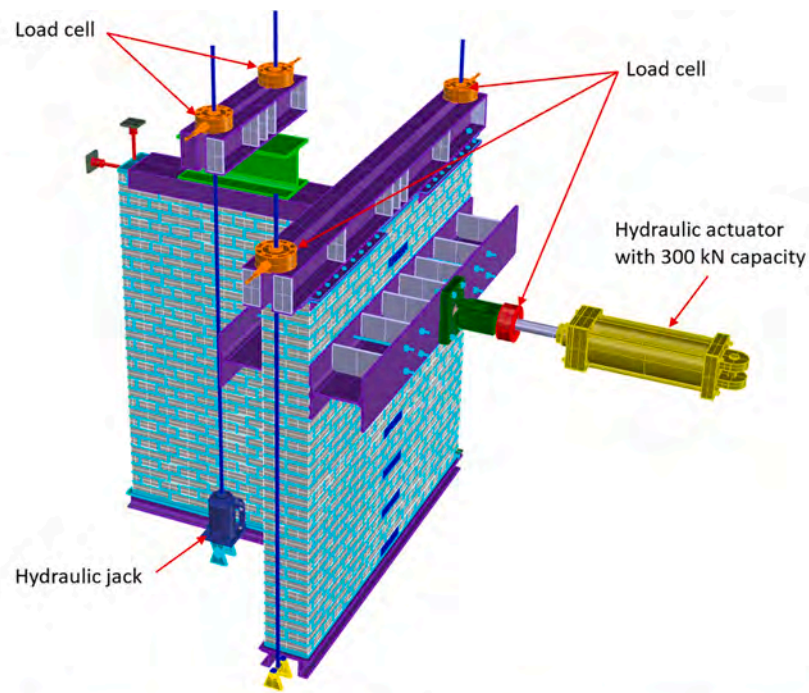
The specimen W2 uplifted up to 4.3 mm in the last part of the test because the 16 twisted bars were able to properly connect the front and back walls, achieving a box-like behavior proved by the rigid body motion of the specimen.

The two retrofitted specimens exhibited different load–displacement behavior due the different number of anchors (Fig. 11).

The specimen W1, retrofitted with 8 twisted bars, was not able to reach the load obtained in the monotonic test. Indeed, the maximum load was 33.3 kN, which was similar to the residual load after first crack appearance of the unreinforced specimen. The vertical prestress on the front and rear walls was almost constant during the whole test (red and green line, Fig. 11a). Conversely, the specimen W2 reached 58.5 kN, with an almost constant prestress in the front wall and a prestress increase on the rear wall. In particular, the specimen uplifted at a level of about 50 kN of the horizontal load, inducing an increase of the prestress. Actually, by reducing the vertical prestress (as shown in the last part of the second test) the horizontal load reduced as well.

It must be noted that, at each displacement level, the residual displacement was noticeable, denoting a high dissipation of the system. This dissipation was associated to a high residual displacement detected in twisted bars. Indeed, as Fig. 12 shows, there was a substantial relative displacement between the outer end of the bar and the front wall. This high displacement was due to a variation of the length of the bar outside the wall (measured on all bars in both specimens), which ranged between 0 mm at the bottom of the wall and 25 mm in the upper areas.

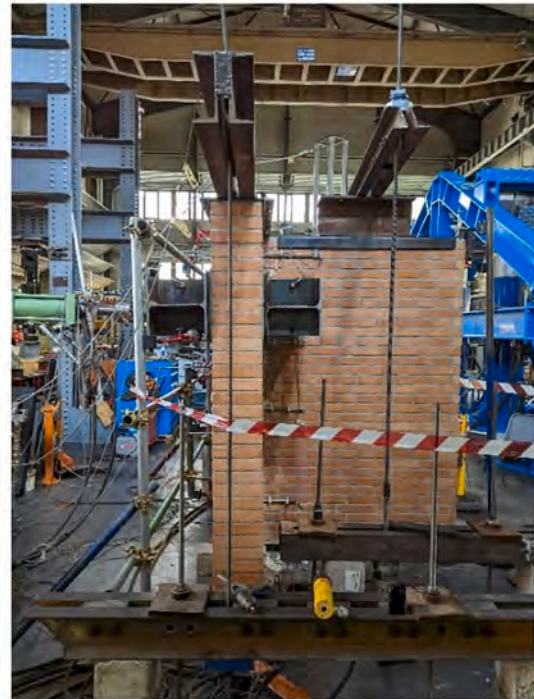
After the full-scale tests, all twisted bars were loaded in a residual pulled-out test according to the procedure described in §2.4 (Fig. 7), and still exhibited a good ductility as shown in Fig. 13. The mean pull-out loads were 7.43 kN (coefficient of variation 9.8 %) and 6.73 kN (coefficient of variation 10.7 %) on specimen W1 and W2, respectively.



(a)



(b)



(c)

Fig. 4. Sketch of test set-up (a), front (b) and side (c) view.

### 3.3. Cyclic test – Post-installed rebar with adhesive reinforcement

After the cyclic tests with the twisted bars, both specimens were retrofitted with 8 post-installed rebars using adhesive, as described in section §2.2 (see Fig. 3a). The final failure crack pattern in both tests was similar, featuring very large cracks with the uplifting of both specimens when the horizontal load reached about 50 kN (Fig. 14), thanks to the ability of this type of connection to achieve a perfect box-like behavior.

Overall, the two specimens exhibited a similar behavior also in terms

of load–displacement curve (Fig. 15), despite the different embedment depth. This similarity is probably due to the good bond of the rear wall. Indeed, with short rebars, a triangular failure was expected (sketch of short ties in Fig. 2), but it was never observed. As for the case of 16 twisted bars, the prestress of the front wall was almost constant (red line), while the prestress of the rear wall started to increase as the horizontal load exceeded about 50 kN (green line).

During the test of specimen W1, the prestress was released several times, and therefore the horizontal load reduced. The maximum load



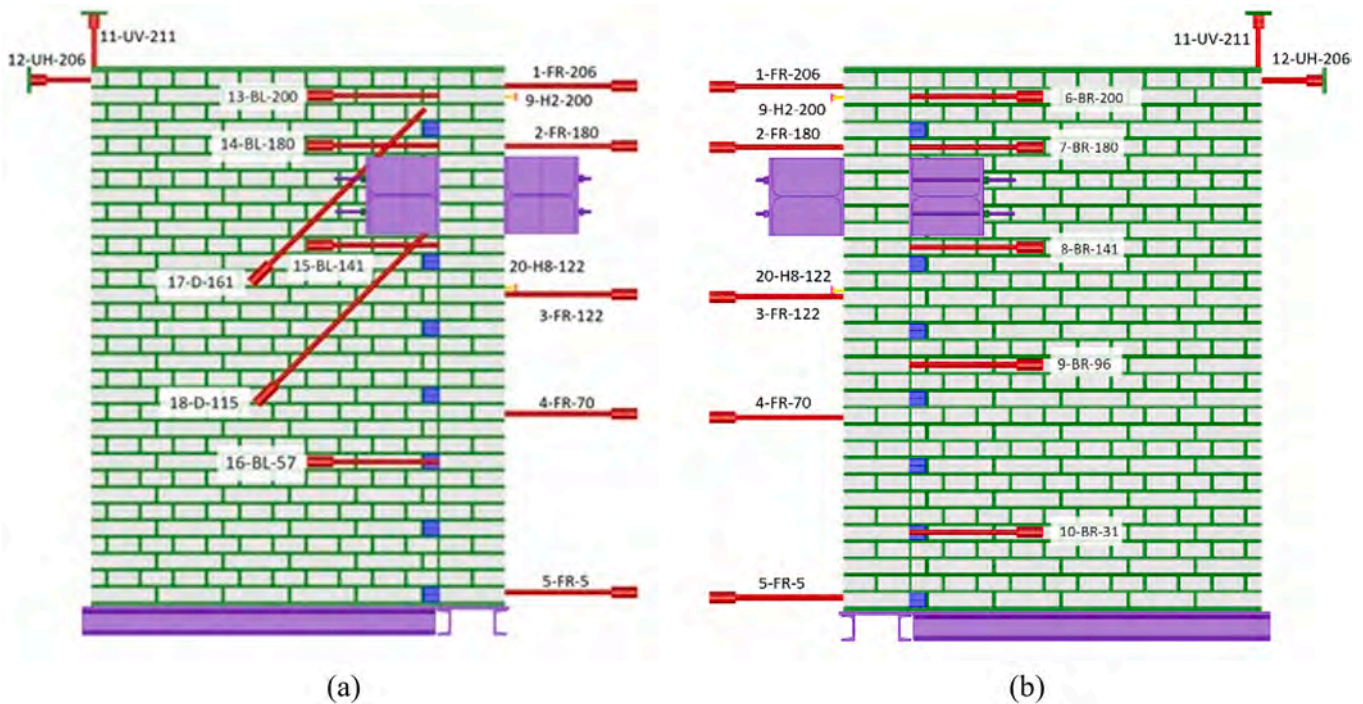


Fig. 5. Left (a) and right (b) view of the position of transducers.

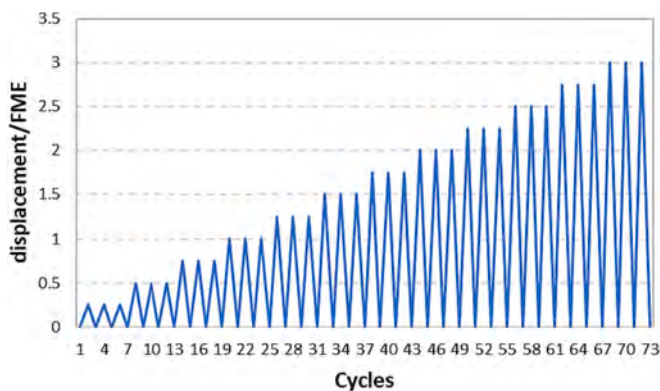


Fig. 6. Test protocol.

reached was 67.6 kN. In case of specimen W2, in the last stage (from a displacement of about 12 mm), the prestress was increased up to 0.3 MPa and the associated maximum horizontal load was 72.3 kN, about 7 % higher than for specimen W1.

#### 4. Discussion

The four retrofitting solutions exhibited different performances both in terms of maximum load and residual displacement/dissipation. Table 2. summarizes the results in terms of maximum horizontal load (correlated to the vertical pressure on the rear wall), maximum displacement at the top of the front wall, and maximum uplift at the back side of the rear wall.

The specimen retrofitted with 8 Heli-Bricks did not uplift significantly (1.8 mm) and it was not possible to reach the maximum load observed in the monotonic test on the URM specimen. This confirmed that rather the 16 twisted bars were needed to properly retrofit the wall, as evaluated in the planning phase of the tests (§2.2). In the other cases, both retrofitting techniques were able to reach a measurable maximum load increase versus the unreinforced specimens.

The specimens with twisted bars exhibited very large displacements and a ductile behavior. This behavior depends on the working mechanism of this type of connection, which derives from: (i) the shape (as per screws), (ii) the mechanical interlock of the wings of the bar in the base material, and (iii) the friction between the lateral surface of the bar and the hole. The high ductility was already observed in previous studies conducted on single twisted bars installed in masonry and subjected to tension, which exhibited a plateau characterized by constant load and large displacements ([35,36]). At the same time, in case of cyclic loads and in the absence of compression, notable residual displacements were observed.

The specimen with post-installed rebars and adhesive achieved a monolithic behavior, with the possibility to meet the “box-like behavior” requirement for the building. Indeed, the uplift of the rear wall reached 13.6 mm, denoting a good connection between the front and the rear wall. This was confirmed by the comparison of the displacements at the top of the wall (Fig. 16).

Considering the absolute displacements of the front (1-FR-206 – red curves) and of the rear walls (12-UH-206 – green curves), and the relative displacement between the front and the rear walls on the right (6-BR-200 – dark-blue curves) and left side (13-BL-200 – light-blue curves), a different behavior of the two retrofitting techniques can actually be observed. The specimens retrofitted with rebars and adhesive (Fig. 16b and Fig. 16d) showed a negligible relative displacement between the front and the rear walls, while the absolute displacements were very close, denoting a rigid motion of the specimen. On the other side, the specimen retrofitted with 8 twisted bars was not able to properly connect the front and the rear walls (Fig. 16a). Indeed, the transducers between the front and the rear walls measured the same displacement as the one on the front wall, denoting a rigid motion of the front wall, detached from the rear wall, which rested on the strong floor. Lastly, the specimen retrofitted with 16 twisted bars was not able to properly connect the front and the rear walls as well (Fig. 16c). Here, also a substantial relative displacement was detected reaching around 80 % of the horizontal absolute displacements of the front wall.

It is interesting to observe that all the solutions did not really show degradation in the cycles at the same displacement level. Indeed, by

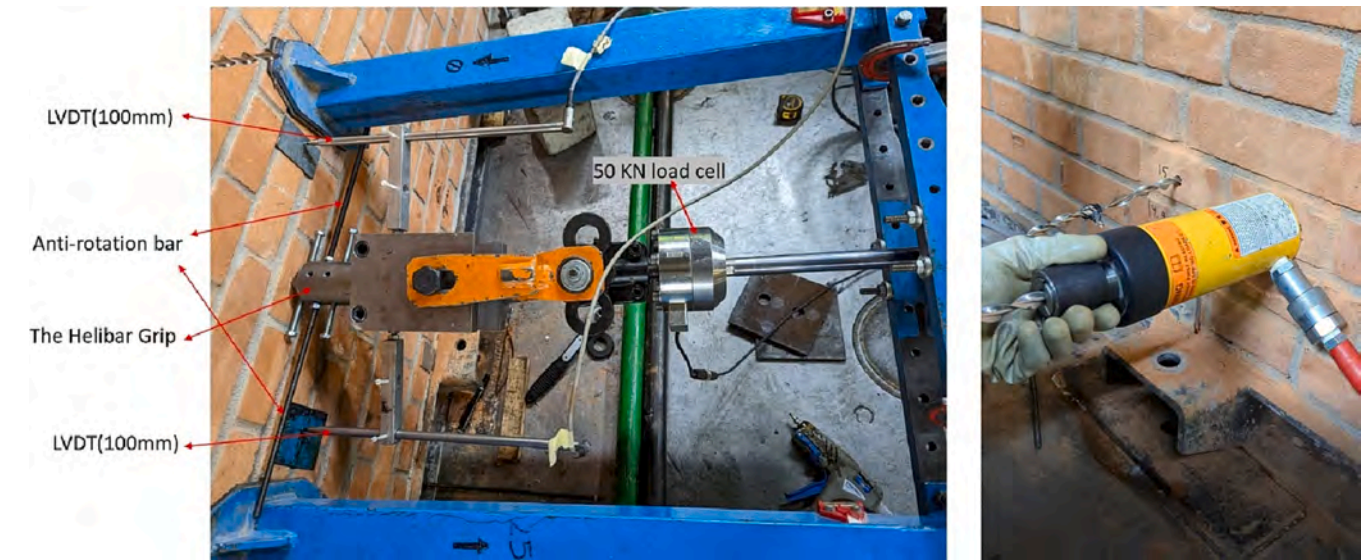


Fig. 7. Twisted bar pull-out test equipment.

**Table 1**  
Summary of the performed tests.

Specimen	1st run	2nd run	3rd run
W1	monotonic until FME	cyclic – 8 Ø12 Heli-Brick	cyclic – 8 Ø12 rebars (85 cm)
W2	monotonic until FME	cyclic – 16 Ø12 Heli-Brick	cyclic – 8 Ø12 rebars (65 cm)

comparing the envelope curves (Fig. 17) of the first (dot), second (square) and third (triangle) cycles within a test series, it can be noted that they are very close. This behavior was already observed by Cattaneo et al. [35] in tension cyclic tests on single bars, and it is probably due to the load transfer mechanism which is governed by the shape of the bar and by the characteristic of the base material.

From the comparison between the cyclic and monotonic test results (Fig. 17), it is interesting to observe that the specimen retrofitted with 8



Fig. 8. Details of the crack between the front and the rear wall.

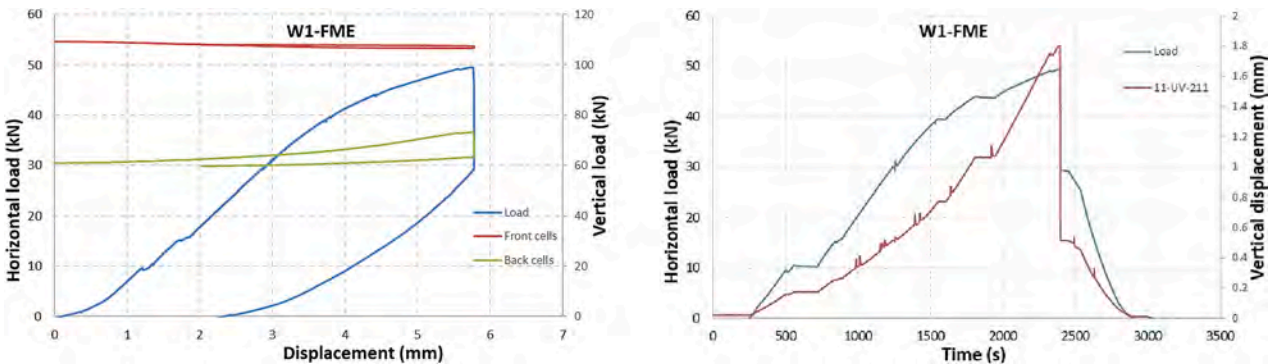


Fig. 9. A) horizontal (left axis) and vertical loads (right axis) vs displacement curves, (b) horizontal load (left axis) and uplift (right axis) vs time curves of the unreinforced specimen.





Fig. 10. Crack pattern after cycles: Specimens W1 (top) and W2 (bottom).

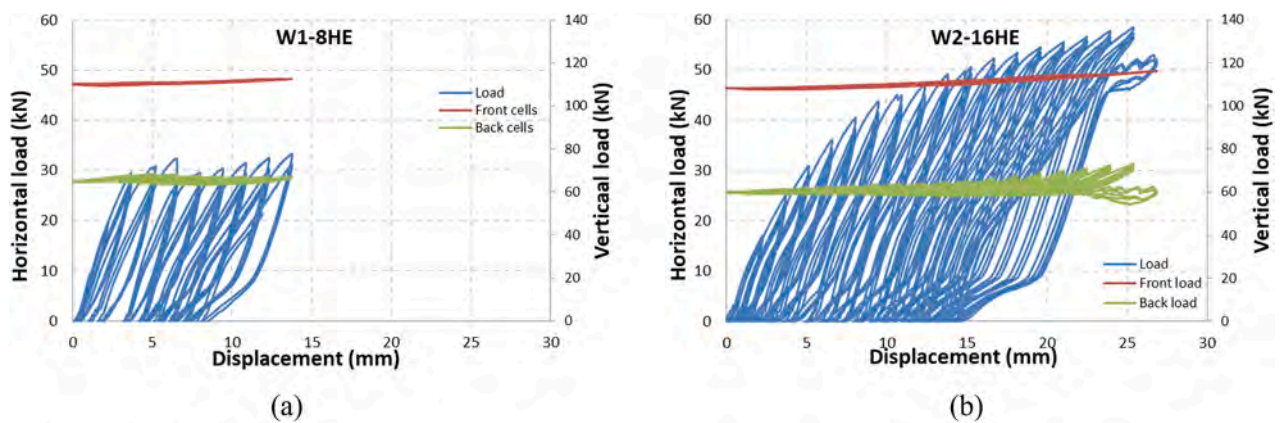


Fig. 11. Horizontal Load (left axis) and vertical load (right axis) vs. displacement curves for the specimen with (a) 8 bars and (b) 16 bars.

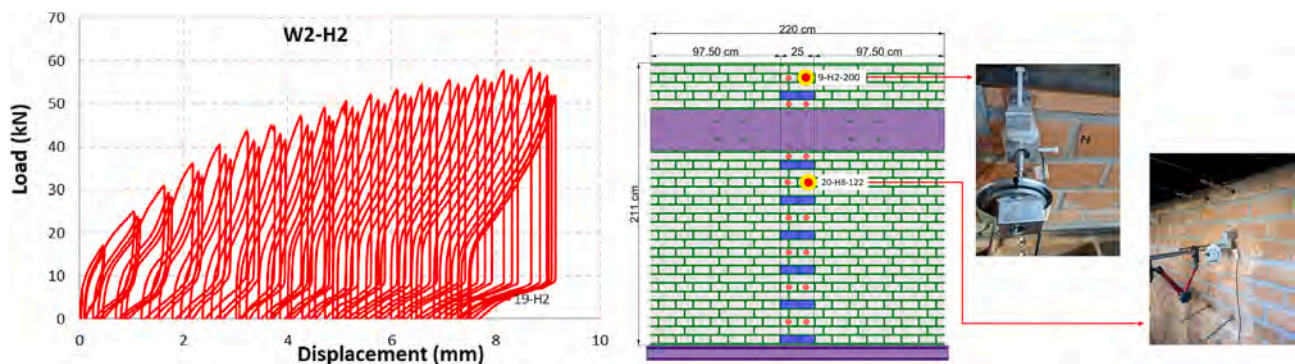


Fig. 12. Displacement of Heli-Brick at the top of the wall.

twisted bars (poor design) was not able to restore the initial capacity of the wall, as expected, while 16 twisted bars (correct design) allowed to improve the initial strength by almost 20 %, with high dissipation and large displacements.

Three possible failure configurations (Fig. 2) were examined to design the reinforcement, considering that the bond pattern between the

two walls was designed weak (Fig. 1) to trigger the failure at the section between the two walls. The first configuration is associated to the failure mechanism shown in Fig. 18a, with the overturning of the front wall subjected to its own weight  $W_1$  and to the prestress load  $P_1$ . No reinforcement is considered and the expected failure load is  $F_1$  (of about 10 kN). The other two failure configurations consider the presence of the



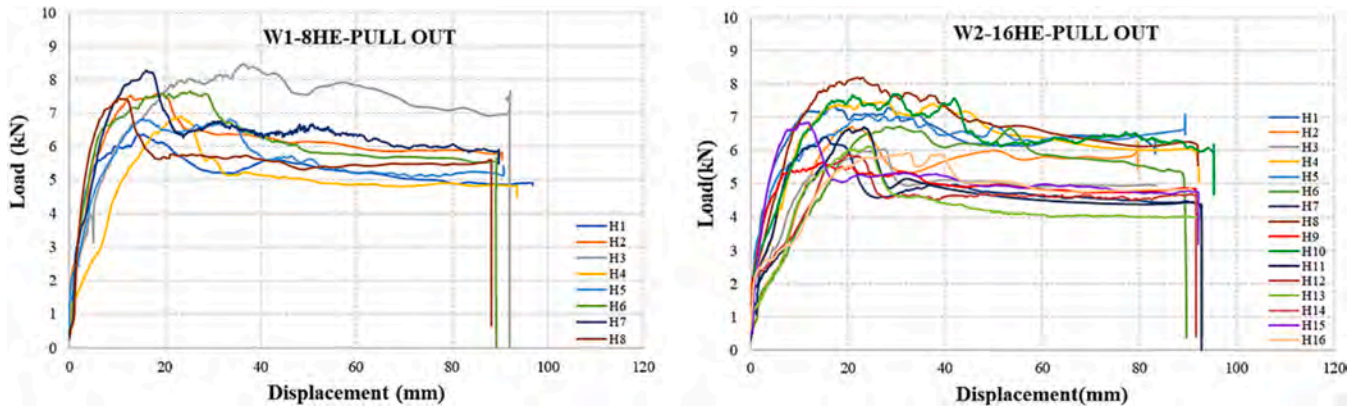


Fig. 13. Residual pull-out tests on twisted bars (first and second wall).



Fig. 14. Crack pattern after cycles and uplift of rear part (specimen W1).

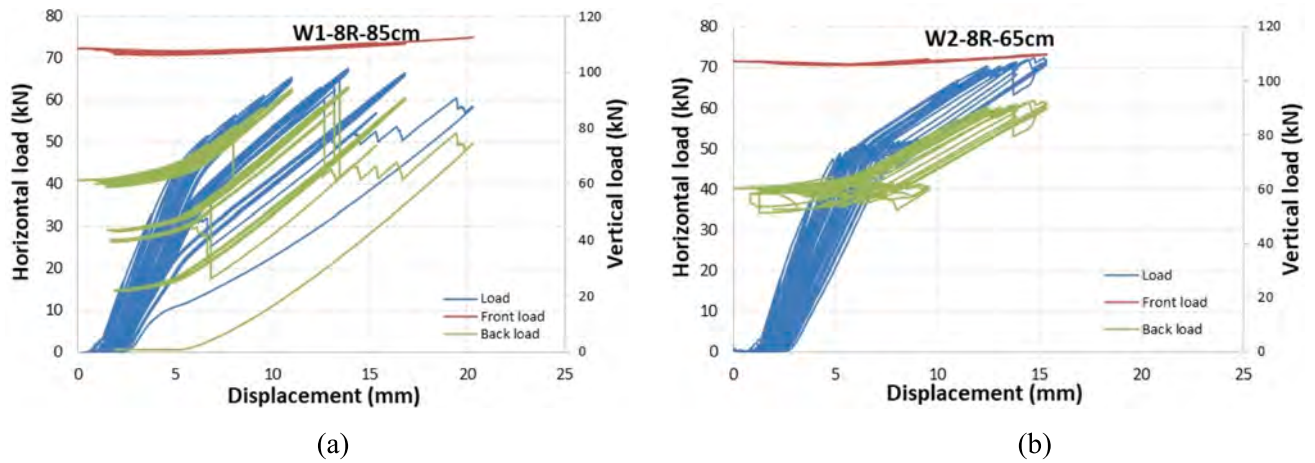


Fig. 15. Horizontal (left axis) and vertical load (right axis) curves, specimen with (a) 85 cm (W1) and (b) 65 cm (W2) embedment length.

**Table 2**  
Summary of test results.

Wall	Twisted bars size 12					8 Rebars $\varnothing 12$ mm				
	# twisted bars	Horizontal load	Vert. rear pressure	Max top displ.	Max uplift	Emb. depth	Horizontal load	Vert. rear pressure	Max top displ.	Max uplift
W1	8	(kN)	(MPa)	(mm)	(mm)	(cm)	(kN)	(MPa)	(mm)	(mm)
W2	16	33.30	0.20	17.9	1.8	85	67.64	0.28*	19.8	13.6
W2	16	58.54	0.21	31.05	4.3	65	52.26	0.19	14.3	9.0
W2	—	—	—	—	—	65	72.34	0.28**	—	—

\*max

\*\*constant

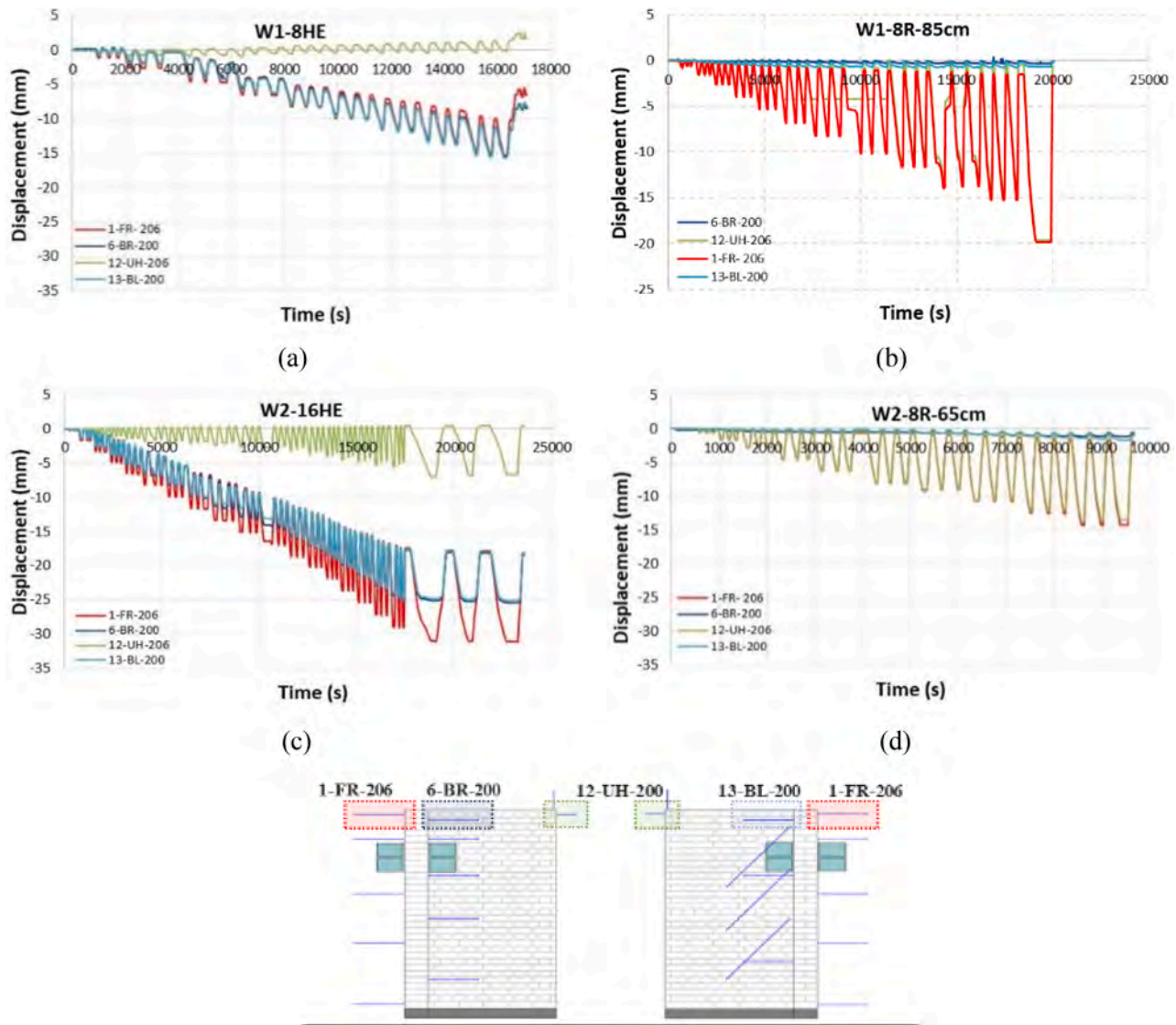


Fig. 16. Time-displacement curves measured at the top of the walls.

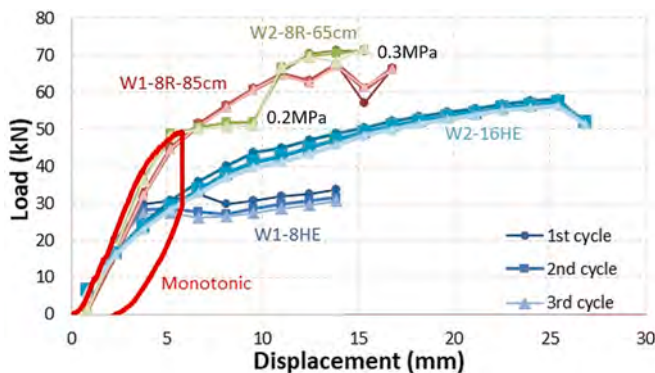


Fig. 17. Envelope load-displacement curves for each cycle vs. monotonic test.

reinforcement and were used to evaluate the necessary number of twisted bars. One is associated to short ties ( $F_2$  of about 45 kN, Fig. 18b), and the other to long ties ( $F_3$  of about 50 kN, Fig. 18c). To achieve the overturning of the whole structure, the connecting bars should be able to sustain the load  $F_3$ - $F_1$ . In the case of twisted bars, the minimum number of required bars was 15, accounting for a design strength of 3 kN for each

bar [35]. Due to symmetry reasons, 16 bars were considered. Consequently, 8 bars were not enough to achieve the monolithic behavior even if, from the displacement point of view, the free rocking of the front wall was partially prevented thanks to the high ductility of the twisted bars. On the contrary, rebars with adhesive, which exhibit higher strength according to the ETA of the product [34] and to the experimental evidence presented by Cattaneo et al. [37], were able to achieve the monolithic behavior considering both a reduced number of bars (i.e. 8 instead of 16) and a reduced embedment length (i.e. 65 instead of 85 cm). This second phenomenon probably was related to the good bond of the rear wall.

The specimens with rebars followed the same behavior of the monotonic tests up to 50 kN, and then they were able to increase the final strength depending on the external pressure, which clearly affects the results as specimen W2-8R-65 cm showed. In both tests, the pressure on the rear wall increased when the horizontal load exceeded about 50 kN. During the test on specimen W2, the pressure was kept constant around 0.2 MPa by releasing the jack pressure during some cycles (horizontal green lines, Fig. 17). Then, the pressure was increased to 0.3 MPa (steep green line), and the horizontal load increased as well. On the contrary, in the specimen W1, where the control of the pressure was more difficult due to the absence of the rear jacks, the horizontal load increased together with the vertical pressure up to a displacement level



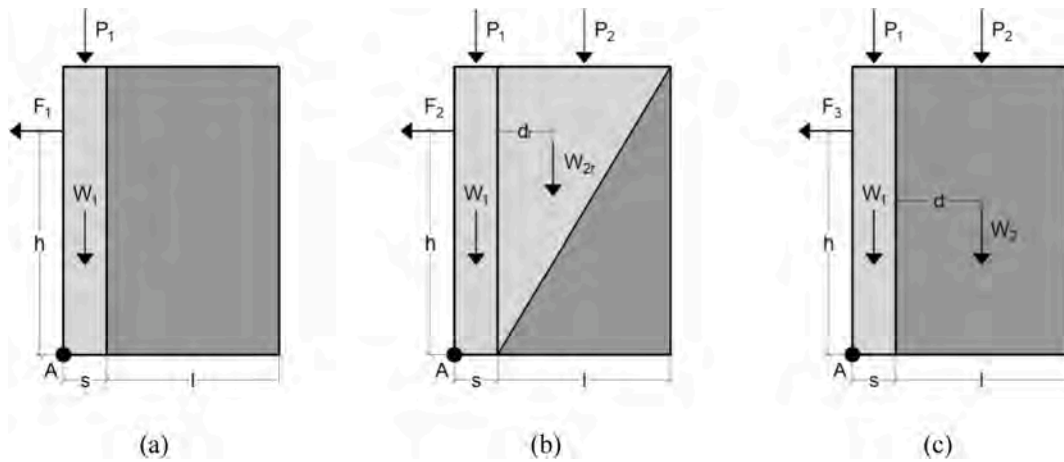


Fig. 18. Failure mechanisms.

of about 12.5 mm. At this displacement level, the rear ties were unscrewed and the rear pressure decreased.

This behavior can be easily explained by imposing the overturning equilibrium of all the loads acting on the walls. In this regard, the sketches of Fig. 18 show the specimen accounting of possible failure mechanisms with the involved loads and lever arms. The walls are subjected to the external horizontal force  $F$  as well as to their self-weight and to the weight of the steel beams, namely  $W_1$  for the front wall (equal to 23.15 kN),  $W_2$  for the back wall (equal to about 14 kN, with a slight difference in the two specimens), and to the vertical prestress  $P_1$  (front load) and  $P_2$  (rear load). In the case of “triangular” failure the self-weight of the rear wall is reduced to  $W_{2r}$ .

By imposing the rocking equilibrium with respect to the point A, the equilibrium load, in the three possible failure configurations, results:

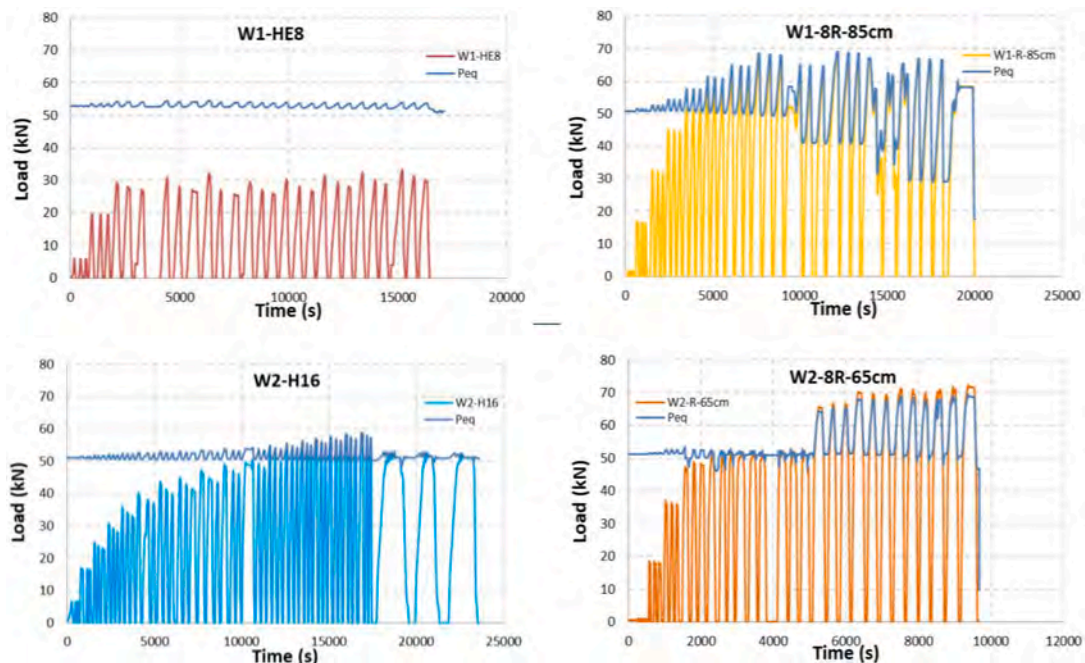
$$F_1 = \frac{(W_1 + P_1) \cdot \frac{s}{2}}{h} \quad (1)$$

$$F_2 = \frac{(W_1 + P_1) \cdot \frac{s}{2} + W_{2r} \cdot \left(s + \frac{l}{3}\right) + P_2 \cdot (s + d)}{h} \quad (2)$$

$$F_3 = P_{eq} = \frac{(W_1 + P_1) \cdot \frac{s}{2} + W_2 \cdot \left(s + \frac{l}{2}\right) + P_2 \cdot (s + d)}{h} \quad (3)$$

where  $s$  is the thickness of the front wall (25 cm),  $l$  is the length of the back wall (137 cm),  $d$  is the distance between the back of the front wall and the axis of application of the vertical prestress  $P_2$  (equal to 69 cm for specimen W1 and to 71 cm for specimen W2), and  $h$  is the height of application of the horizontal load from the strong floor (1.72 m).

By assuming roughly  $P_1 = 110$  kN and  $P_2 = 60$  kN, the equilibrium load  $P_{eq}$  results in 50.07 kN and 51.18 kN for the first (W1) and second (W2) specimen, respectively. By evaluating the horizontal load  $P_{eq}$  assuming the actual loads  $P_1$  and  $P_2$  measured by the load cells, the load vs time graphs reported in Fig. 19 for  $P_{eq}$  are obtained for both specimens and both retrofitting methods (dark blue curves). For comparison,

Fig. 19. Jack load and horizontal equilibrium load  $P_{eq}$  vs time.

the actual applied horizontal load in each test is also given. It can be noted that in test W1-8HE the applied load (red curve) never reaches  $P_{eq}$ , while in all the other tests, once the load reached about 50 kN,  $P_{eq}$  and the applied load are about identical and, due to the rigid body motion of the specimen, the load can be increased only if the prestresses  $P_1$  and  $P_2$  are increased. Thus, for the considered specimen and the applied prestress, the “limit” load was 50 kN.

In the case of 8 twisted bars, the retrofitting solution was not able to achieve that load, while the other solutions were strong enough to guarantee the monolithic (rebar) or almost monolithic (16 twisted bars) behavior of the specimen. The results show that the number of twisted bars evaluated at the beginning (16) resulted suitable to guarantee the stability of the front wall against the rocking. However, even if the rotation equilibrium requirement seems appropriate for the design of the number of bars, it should be highlighted that the evaluation of the optimal number is strictly related to the bonding between the front and the rear wall as well as the vertical load applied on the wall.

## 5. Conclusions

An experimental program has been carried out to investigate the influence of different retrofitting solutions on the load bearing behavior of unreinforced poorly connected orthogonal masonry walls. Two clay brick T-shaped masonry walls were tested considering two strengthening techniques for the T-connection, either using stainless steel twisted bars or steel rebars with injection mortar. The masonry specimens were subjected to constant vertical loads and horizontal increasing displacements. Each unreinforced specimen was monotonically tested until the first crack (associated to the FME) was detected. Then, after installation of the retrofitting solutions, cyclic testing was performed in two consecutive runs, to investigate the effectiveness of the two different retrofitting techniques.

The results showed that the strengthening solution with twisted bars significantly improved the dissipation capacity of the specimen, with symmetric behavior on the left and right side of the specimen. However, the 8 Heli-Bricks configuration was not able to restore the initial capacity of the unreinforced wall (i.e., the load associated with the FME was not reached), while the 16 Heli-Bricks configuration allowed to improve the initial strength, with high dissipation and large displacements. Nevertheless, a noticeable relative displacement between the front and the back of the wall was evident in this last case.

The retrofitting method with rebars and injection mortar showed higher resistance, but a less ductile and dissipative behavior with respect to the twisted bars solution. Furthermore, a perfect monolithic behavior was evident, proved by the uplift of the rear wall that reached 13.6 mm. The variation of the embedment depth from 85 cm to 65 cm did not show any significant effect on the results indicating that the shallower embedment was sufficient to properly transfer the acting forces.

It should be noted that the vertical prestress applied on the rear wall significantly affected the horizontal load. Indeed, after a certain value, it was not possible to increase the horizontal load anymore if the vertical pressure was not increased as well. Once the pressure was increased, the horizontal load increased too in correlation with a clear change of the system's stiffness.

Overall, both retrofitting techniques, when properly designed, showed their capability to restore the initial capacity of the wall, with different crack amplitudes and displacements, and different levels of stiffness and dissipation as well. However, it must be underlined that twisted bars have a great potential in the retrofitting of historical buildings thanks to their better compatibility with masonry structures, since no adhesives are required.

This paper is a first attempt to assess the structural behavior of twisted bars, and showed that the high ductility observed in pull-out test is confirmed also at the structural level. However, additional researches should be performed in order to cover all possible applications, considering, as example, different geometries of the connection.

## Declaration of Competing Interest

The authors declare that they have no known competing financial interests or personal relationships that could have appeared to influence the work reported in this paper.

## Data availability

The authors do not have permission to share data.

## References

- [1] Ministero dei Lavori Pubblici. Legge n. 64 del 2 Febbraio 1974 - Provvedimenti per le costruzioni con particolari prescrizioni per le zone sismiche 1974.
- [2] Ministero dei Lavori Pubblici. Decreto Ministero dei Lavori Pubblici 2 Luglio 1981 - Normativa per le riparazioni ed il rafforzamento degli edifici danneggiati dal sisma nelle regioni Basilicata, Campania e Puglia 1981.
- [3] G. Vlachakis, E. Vlachaki, P.B. Lourenço, Learning from failure: damage and failure of masonry structures, after the Lesvos earthquake (Greece), Eng. Fail. Anal. 2020 (2017) 117.
- [4] D. Perrone, P.M. Calvi, R. Nascimbene, E.C. Fischer, G. Magliulo, Seismic performance of non-structural elements during the Central Italy earthquake, Bull. Earthq. Eng. 2019 (2016) 17, <https://doi.org/10.1007/s10518-018-0361-5>.
- [5] Işık E, Avcil F, Büyüksaraç A, İzol R, Hakan Arslan M, Aksoylu C, et al. Structural damages in masonry buildings in Adıyaman during the Kahramanmaraş (Türkiye) earthquakes (Mw 7.7 and Mw 7.6) on 06 February 2023. Eng Fail Anal 2023;151. <https://doi.org/10.1016/j.engfailanal.2023.107405>.
- [6] Penna A, Calderini C, Sorrentino L, Carocci CF, Cescatti E, Sisti R, et al. Damage to churches in the 2016 central Italy earthquakes. Bulletin of Earthquake Engineering 2019;17. <https://doi.org/10.1007/s10518-019-00594-4>.
- [7] G. de Felice, R. Fugger, F. Gobbin, Overturning of the façade in single-nave churches under seismic loading, Bull. Earthq. Eng. 20 (2022), <https://doi.org/10.1007/s10518-021-01243-5>.
- [8] P.B. Lourenço, N. Mendes, L.F. Ramos, D.V. Oliveira, Analysis of masonry structures without box behavior, International Journal of Archit. Herit. 5 (2011), <https://doi.org/10.1080/15583058.2010.528824>.
- [9] S. Bhattacharya, S. Nayak, S.C. Dutta, A critical review of retrofitting methods for unreinforced masonry structures, Int. J. Disaster Risk Reduct. 7 (2014) 51–67, <https://doi.org/10.1016/j.ijdrr.2013.12.004>.
- [10] R. Capozucca, E. Magagnoli, Experimental response of masonry walls in-plane loading strengthened with GFRP strips, Compos. Struct. 235 (2020), <https://doi.org/10.1016/j.compstruct.2019.111735>.
- [11] L. Bionzi, S. Cattaneo, P. Crespi, M. Scamardo, N. Vafa, Diagonal compression cyclic testing of unreinforced and reinforced masonry walls, Constr. Build. Mater. 363 (2023).
- [12] Wang C, Sarhosis V, Nikitas N. Strengthening/Retrofitting Techniques on Unreinforced Masonry Structure/Element Subjected to Seismic Loads: A Literature Review. The Open Construction and Building Technology Journal 2018;12. <https://doi.org/10.2174/1874836801812010251>.
- [13] F. Yavartanoo, T.H.K. Kang, Retrofitting of unreinforced masonry structures and considerations for heritage-sensitive constructions, Journal of Building Engineering 49 (2022), 103993, <https://doi.org/10.1016/J.JOBE.2022.103993>.
- [14] P. Meriggi, G. de Felice, S. De Santis, Design of the out-of-plane strengthening of masonry walls with fabric reinforced cementitious matrix composites, Constr. Build. Mater. 240 (2020), 117946, <https://doi.org/10.1016/J.CONBUILDMAT.2019.117946>.
- [15] G. Maddaloni, M. Di Ludovico, A. Balsamo, A. Prota, Out-of-plane experimental behaviour of T-shaped full scale masonry wall strengthened with composite connections, Compos. B Eng. 93 (2016) 328–343, <https://doi.org/10.1016/J.COMPOSITESB.2016.03.026>.
- [16] Longarini N, Crespi P, Franchi A, Giordano N, Ronca P, Scamardo M. Cross-lam roof diaphragm for the seismic retrofitting of historical masonry churches. Proceedings of the International Masonry Society Conferences, vol. 0, 2018.
- [17] F. Ceroni, H. Darban, N. Caterino, R. Luciano, Efficiency of injected anchors in masonry elements: Evaluation of pull-out strength, Constr. Build. Mater. 267 (2021), <https://doi.org/10.1016/j.conbuildmat.2020.121707>.
- [18] A. Cascardi, M. Leone, M.A. Aiello, Transversal joining of multi-leaf masonry through different types of connector: experimental and theoretical investigation, Constr. Build. Mater. 265 (2020), <https://doi.org/10.1016/J.CONBUILDMAT.2020.120733>.
- [19] S. Paganoni, D. D'Ayala, Testing and design procedure for corner connections of masonry heritage buildings strengthened by metallic grouted anchors, Eng. Struct. 70 (2014) 278–293, <https://doi.org/10.1016/J.ENGSTRUCT.2014.03.014>.
- [20] E. Vintzileou, I. Tselios, G. Welz, D. Karagiannaki, Anchors to Masonry in Seismic Conditions: Cracked vs. Uncracked Locations (2023), [https://doi.org/10.1007/978-3-031-32511-3\\_29](https://doi.org/10.1007/978-3-031-32511-3_29).
- [21] A. Maione, C. Casapulla, M. Di Ludovico, A. Prota, F. Ceroni, Efficiency of injected anchors in connecting T-shaped masonry walls: a modelling approach, Constr. Build. Mater. 301 (2021), <https://doi.org/10.1016/j.conbuildmat.2021.124051>.
- [22] M. Corradi, A. Di Schino, A. Borri, R. Rufini, A review of the use of stainless steel for masonry repair and reinforcement, Constr. Build. Mater. 181 (2018), <https://doi.org/10.1016/j.conbuildmat.2018.06.034>.



- [23] N. Ismail, J.M. Ingham, In-situ and laboratory based out-of-plane testing of unreinforced clay brick masonry walls strengthened using near surface mounted twisted steel bars, *Constr. Build. Mater.* 36 (2012), <https://doi.org/10.1016/j.conbuildmat.2012.04.087>.
- [24] C. Gentilini, F. Finelli, C. Carloni, An experimental study of the bond behavior of twisted steel bars embedded in mortar cylinders and in the joints of masonry wallettes, *Constr. Build. Mater.* 316 (2022), <https://doi.org/10.1016/j.conbuildmat.2021.125795>.
- [25] EOTA. EAD 330076-01-0604-v01: Metal injection anchors for use in masonry under seismic actions. Brussels, Belgium: 2022.
- [26] EOTA. TR 53: Recommendations for tests of metal injection anchors for use in masonry to be carried out on construction works. Technical Report. Brussels, Belgium: 2016.
- [27] EOTA. TR 054: Design methods for anchorages with metal injection anchor and screw anchors for use in masonry. Technical Report. . Brussels, Belgium: 2016.
- [28] ASTM C67/C67M-21, *Standard Test Methods for Sampling and Testing Brick and Structural Clay Tile*. ASTM, International (2021).
- [29] ASTM C1006-13. *Standard Test Method for Splitting Tensile Strength of Masonry Units*. vol. 07. 2013.
- [30] Bs, *Testing Concrete - Part 117: Method for determination of tensile splitting strength*, *British Standard Institution* 1983 (2) (1881–117.).
- [31] C348 – 21. *Standard Test Method for Flexural Strength of Hydraulic-Cement Mortars*. Annual Book of ASTM Standards 2021;!
- [32] ASTM C109/C109M-02. *Standard Test Method for Compressive Strength of Hydraulic Cement Mortars*. Annual Book of ASTM Standards 2020;04.
- [33] Hilti Italia S.p.A. Hilti Heli-Brick documentation and instructions for use n.d.
- [34] ETA-22/0395. Hilti Injection system HIT-HY 270 in solid bricks. Metal Injection anchors for use in masonry. 2022.
- [35] S. Cattaneo, M. Scamardo, Assessment of the tensile behavior of twisted steel connectors for masonry retrofitting, *Constr. Build. Mater.* 392 (2023), <https://doi.org/10.1016/j.conbuildmat.2023.131771>.
- [36] Gentilini C, Finelli F, Girelli VA, Franzoni E. Pull-out behavior of twisted steel connectors employed in masonry: The influence of the substrate. *Constr Build Mater* 2021;274. <https://doi.org/10.1016/J.CONBUILDMAT.2020.122115>.
- [37] S. Cattaneo, N. Vafa, Tensile capacity of adhesive anchors in damaged masonry, *Applied Sciences (switzerland)* 11 (2021), <https://doi.org/10.3390/app112110135>.